A fatty acid-binding protein of *Streptococcus pneumoniae* facilitates the acquisition of host polyunsaturated fatty acids

Received for publication, August 14, 2019, and in revised form, September 16, 2019 Published, Papers in Press, September 17, 2019, DOI 10.1074/jbc.RA119.010659

Jessica M. Gullett[‡], **Maxime G. Cuypers**[§], **Matthew W. Frank**[‡], **Stephen W. White**[§], **and Charles O. Rock**[‡1]

From the Departments of [‡]*Infectious Diseases and* [§]*Structural Biology, St. Jude Children's Research Hospital, Memphis, Tennessee 38105*

Edited by George M. Carman

Streptococcus pneumoniae **is responsible for the majority of pneumonia, motivating ongoing searches for insights into its physiology that could enable new treatments.** ***S. pneumoniae*** **responds to exogenous fatty acids by suppressing its** ***de novo*** **biosynthetic pathway and exclusively utilizing extracellular fatty acids for membrane phospholipid synthesis. The first step in exogenous fatty acid assimilation is phosphorylation by fatty acid kinase (FakA), whereas bound by a fatty acid-binding protein (FakB).** ***Staphylococcus aureus*** **has two binding proteins, whereas** ***S. pneumoniae*** **expresses three. The functions of these binding proteins were not clear. We determined the** ***Sp*****FakB1- and** ***Sp*****FakB2-binding proteins were bioinformatically related to the two binding proteins of** ***Staphylococcus aureus*****, and biochemical and X-ray crystallographic analysis showed that** ***Sp*****FakB1 selectively bound saturates, whereas** ***Sp*****FakB2 allows the activation of monounsaturates akin to their** ***S. aureus*** **counterparts. The distinct** ***Sp*****FakB3 enables the utilization of polyunsaturates. The** ***Sp*****FakB3 crystal structure in complex with linoleic acid reveals an expanded fatty acid-binding pocket within the hydrophobic interior of** ***Sp*****FakB3 that explains its ability to accommodate multiple** ***cis*** **double bonds.** ***Sp*****FakB3 also utilizes a different hydrogen bond network than other FakBs to anchor the fatty acid carbonyl and stabilize the protein.** ***S. pneumoniae*** **strain JMG1 (Δ*fakB3*) was deficient in incorporation of linoleate from human serum verifying the role of FakB3 in this process. Thus, the multiple FakBs of** ***S. pneumoniae*** **permit the utilization of the entire spectrum of mammalian fatty acid structures to construct its membrane.**

The ability to acquire exogenous fatty acids (FA)[2] for membrane phospholipid synthesis is a universal feature of lipid metabolism in Firmicutes, a phylum of Gram-positive bacteria that contains many important human pathogens. The first step in FA incorporation is activation by FA kinase, an enzyme system consisting of a kinase domain protein (FakA) that phosphorylates a FA carried by the FA-binding protein component (FakB) (1). The resulting acyl-phosphate (FA∼P) bound to FakB is either transferred to the glycerol phosphate acyltransferase (PlsY) to initiate phospholipid synthesis or transferred to acyl carrier protein (ACP) by PlsX (2). The resulting acyl-ACP is either utilized by PlsC to acylate the 2-position of 1-acylglycerolphosphate or it may enter the FASII cycle and be elongated. The elongated acyl-ACP is then metabolized via PlsX/PlsY or PlsC like the acyl-ACP derived from *de novo* biosynthesis. Two major orders of the Firmicutes have distinctly different physiological responses to the presence of extracellular FA. The Bacillales, exemplified by *Staphylococcus aureus*, do not genetically suppress the genes of type II FA biosynthesis (FASII) in the presence of exogenous FA (3). Rather, FASII continues to produce primarily *anteiso*15:0 that is placed in the 2-position, and the exogenous long-chain saturated and monounsaturated FA are activated by FA kinase and placed into the 1-position (4, 5). The Lactobacillales, exemplified by *Streptococcus pneumoniae*, have a different response. These organisms strongly suppress the expression of the genes encoding the FASII enzymes in response to exogenous FA. This response is mediated by the FabT transcriptional repressor (6–9). FabT bound to acyl-ACP tightly binds to promoters within the FASII gene cluster to potently suppress FASII gene expression (10). Thus, these organisms construct their membrane phospholipids almost exclusively using FA obtained from the environment to acylate both positions of the glycerol-phosphate backbone (3, 11). Elongation is not a significant fate for exogenous FA in the Lactobacillales because the FabT system suppresses the transcription of the entire gene set responsible for the FASII elongation cycle.

The ability of FA kinase to activate FA encountered in the environment is conferred by the FA selectivities of the FakB component. *S. aureus* expresses two FakBs (1, 5). *Sa*FakB1 is specific for saturated FA (16:0), whereas *Sa*FakB2 selectively binds monounsaturated FA (18:1) (1, 5, 12). *S. aureus* does not synthesize unsaturated FA, so *Sa*FakB1 is the housekeeping protein and *Sa*FakB2 is responsible for the uptake of host monounsaturated FA (1, 5, 12). *S. pneumoniae* encodes three

This work was supported by National Institutes of Health Grant GM034496, Cancer Center Support Grant CA21765, and the American Lebanese Syrian Associated Charities. The authors declare that they have no conflicts of interest with the contents of this article. The content is solely the responsibility of the authors and does not necessarily represent the official views of the National Institutes of Health.

The atomic coordinates and structure factors (codes 6NOK, 6DKE, 6DJ6, 6NR1, and 6CNG) have been deposited in the Protein Data Bank (http://wwpdb.org/).

[1] To whom correspondence should be addressed: Dept. of Infectious Diseases, St. Jude Children's Research Hospital, 262 Danny Thomas Place, Memphis, TN 38105. Tel.: 901-595-3491; E-mail: Charles.rock@stjude.org.

[2] The abbreviations used are: FA, fatty acid; FA∼P, acyl-phosphate; ACP, acyl carrier protein; FASII, bacterial type II fatty acid biosynthesis pathway; *a*15:0, *anteiso* pentadecanoic acid; LPA, 1-acyl-*sn*-glycerol-3-phosphate; PlsX, acyl-phosphate:ACP transacylase; PlsY, acyl-phosphate-dependent glycerol-phosphate acyltransferase; PG, phosphatidylglycerol; PDB, Protein Data Bank; CAPSO, 3-(cyclohexylamino)-2-hydroxy-1-propanesulfonic acid.

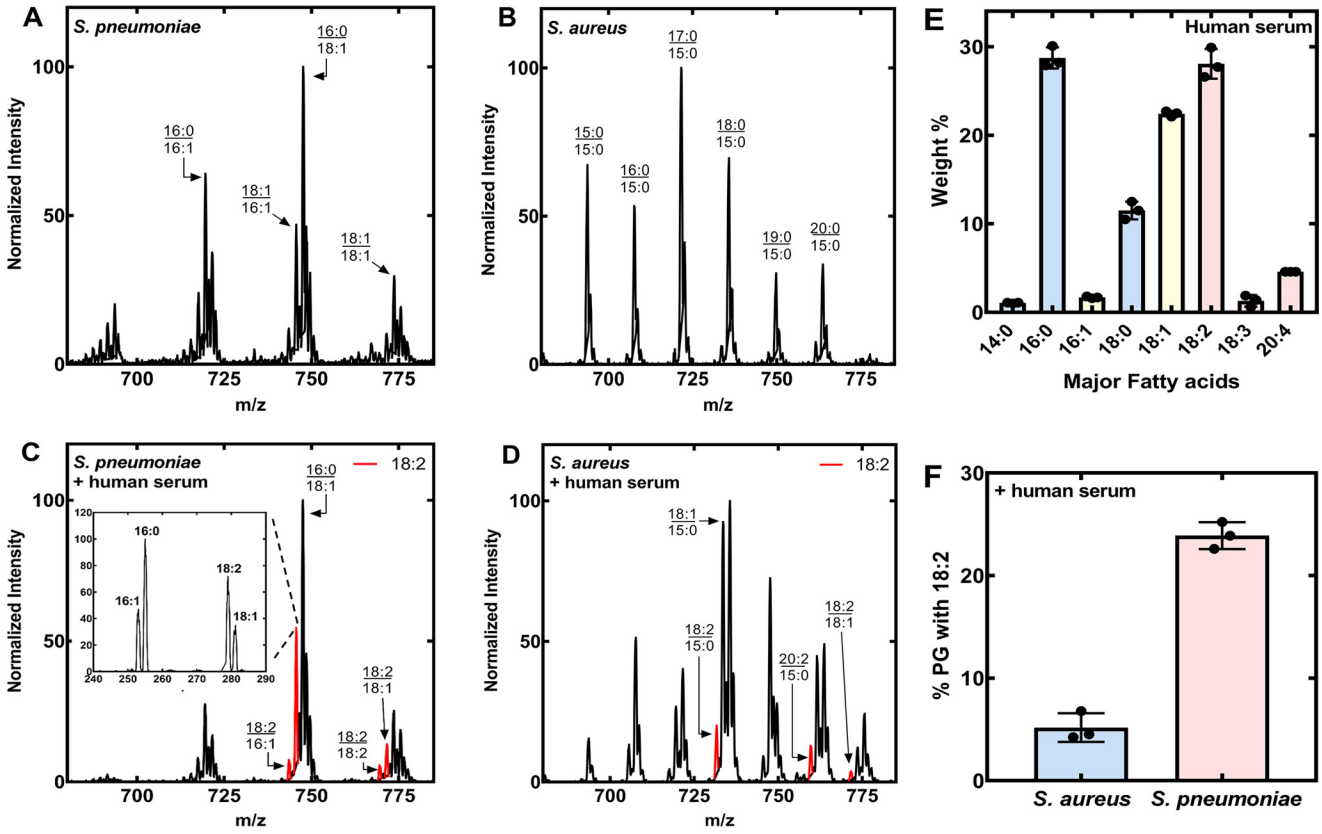

Figure 1. PG molecular species in the presence and absence of human serum. *S. pneumoniae* strain TIGR4 and *S. aureus* strain AH1263 were grown in their respective medium or in medium:human serum (1/1, v/v). The PG molecular species were determined under each of the four culture conditions in triplicate, and representative spectra are shown. The molecular species that contain an 18:2 or 18:2-derived FA are highlighted in *red*. *A*, *S. pneumoniae* grown in C+Y media. *B*, *S. aureus* grown in Luria broth. *C*, *S. pneumoniae* grown with 50% human serum, 50% C+Y medium. The presence of 18:2 in the $m/z = 745$ peak was verified by fragmentation (*inset*). *D*, *S. aureus* grown with 50% human serum, 50% Luria broth. *E*, major FA of human serum. Lipids were extracted from triplicate samples of human serum and the total FA composition determined by GC of the derived methyl esters. The weight percent of each FA was calculated. FA less than 1% of the total are not shown. *F*, triplicate biological replicates were obtained, the areas under each peak in the spectra were summed, and the PG molecular species containing 18:2 as a percent of the total area were calculated to provide an estimate of 18:2 incorporation. Peaks containing elongation products, like 20:2 derived from 18:2, were included in the calculation for the contribution of the parent FA.

FakB-binding proteins suggesting an expanded repertoire of FA-binding capabilities to enable the acquisition of environmental FA to replace *de novo* biosynthesis. Here, we report that two of these binding proteins, *Sp*FakB1 and *Sp*FakB2, are bioinformatically related to the two FakBs previously characterized in *S. aureus* (5, 12). Heterologous expression, biochemical analyses, and X-ray crystallography confirmed that *Sp*FakB1 specifically bound saturated FA (16:0) and *Sp*FakB2 selectively bound monounsaturated FA (18:1) but also bound saturated FA. Fatty acids are designated by number of carbons:number of double bonds. *Sp*FakB3 is more distantly related to the *S. aureus* homologs, and heterologous expression and biochemical analyses showed that *Sp*FakB3 expanded the repertoire of substrates to polyunsaturated FA (18:2). The *Sp*FakB3(18:2) structure revealed a different hydrogen bond network anchoring the FA carbonyl and an expanded FA-binding pocket within the hydrophobic interior of the protein that explains its ability to bind FA with multiple *cis* double bonds. *S. pneumoniae* strain JMG1 (Δ*fakB3*) was deficient in 18:2 incorporation verifying the role of *Sp*FakB3 in the incorporation of polyunsaturated FA into *S. pneumoniae* phospholipids. Thus, the multiple FakBs of *S. pneumoniae* permit the acquisition and utilization of the entire spectrum of mammalian FA structures to facilitate the acquisition of host FA to construct its membrane at the infection site.

Results

Incorporation of FA from human serum

The distinct difference between *S. aureus* and *S. pneumoniae* utilization of exogenous FA is illustrated by the effect of human serum supplementation on the molecular species composition of PG, a major membrane phospholipid in both organisms (Fig. 1). *S. pneumoniae* FASII produced both saturated and monounsaturated FA when grown in C+Y medium without FA supplement (3) (Fig. 1*A*). The two most abundant PG molecular species had 16:0 paired with either 16:1 or 18:1. *S. pneumoniae* is like most organisms in that it places saturated FA in the 1-position and unsaturated FA in the 2-position of its membrane phospholipids (13). *S. aureus* places *anteiso*15:0 in the 2-position of the glycerol backbone (3) giving rise to *S. aureus* PG molecular species with only saturated, straight, and branched-chain FA paired with *anteiso*15:0 when grown in media without exogenous FA (Fig. 1*B*). These data illustrate the difference in membrane phospholipid structures produced by *de novo* biosynthesis in these two Gram-positive pathogens.

Both *S. pneumoniae* and *S. aureus* incorporated FA derived from serum lipids when cultured in the presence of human serum. The *S. pneumoniae* PG molecular species pattern when grown in human serum was different from the pattern obtained in the absence of an exogenous lipid supplement (Fig. 1*C*). The most abundant peak, $m/z = 747$, corresponded to a 16:0/18:1 in both growth conditions, and in the presence of human serum the 16:0/16:1 peak was less prominent. This pattern is consistent with the observation that *S. pneumoniae* shuts down *de novo* lipid synthesis when supplied with an exogenous source of FA (3). Peaks in the spectrum arising from the synthesis of molecular species containing 18:2 are highlighted in *red* (Fig. 1*C*). A major new peak ($m/z = 745$) was fragmented to verify that 16:0/18:2 was the most abundant molecular species at this mass position (Fig. 1*C*, *inset*). *S. pneumoniae* cannot make 18:2, thus this FA must be derived from the human serum. The origin of the saturated and monounsaturated FA in PG cannot be unambiguously determined in this experiment because these FA are synthesized by *S. pneumoniae* and are present in human serum. The analysis of *S. aureus* grown with human serum showed that most PG molecular species still contained 15:0, but that 18:1 along with its elongation product 20:1 were incorporated from the serum (Fig. 1*D*). Human serum contains nonesterified FA plus an abundance of glycerolipids, and both *S. aureus* (*geh* and *lip*) (14) and *S. pneumoniae* (*lipA*) (15) express genes capable of hydrolyzing these lipids to release FA. The three most abundant FA in the human serum sample used in our study were 16:0, 18:1, and 18:2 (Fig. 1*E*). Although 18:1 and 18:2 were about equal in abundance, *S. aureus* incorporated significantly more 18:1 than 18:2 (Fig. 1*D*). The incorporation of 18:2 into PG was significantly less in *S. aureus* compared with the more robust incorporation of 18:2 into the *S. pneumoniae* lipidome (Fig. 1*F*). These data indicated that *S. pneumoniae* had a higher capacity to extract polyunsaturated FA from human serum than *S. aureus*.

Three fakB genes in S. pneumoniae

S. aureus expresses two FakB proteins, one specific for saturated FA and the other specific for monounsaturated FA (5). The fact that *S. pneumoniae* incorporates 18:2 into its phospholipids suggested that it had a FA-binding protein capable of binding polyunsaturated FA. We identified a single *fakA* gene (locus tag: Sp0443) and 3 *fakB* genes (locus tags: Sp1557, Sp1112, Sp0742) in the *S. pneumoniae* TIGR4 genome. The protein sequences were compared using BLASTP alignment software using the KEGG database sequence entries. The Sp1557 gene was named *fakB1* because it encoded a protein that was 35% identical to *Sa*FakB1 and 29% identical to *Sa*FakB2. The Sp1112 gene was named *fakB2* because it encoded a protein with 29% identity to *Sa*FakB2 and 28% identity to *Sa*FakB1. The Sp0742 gene encoded a protein that was the least similar to the *S. aureus* FakBs (18% to *Sa*FakB1 and 26% to *Sa*FakB2), and it was designated *fakB3*. Both *S. pneumoniae* and *S. aureus* are in the phylum Firmicutes and class Bacilli, but *S. pneumoniae* is in the Order Lactobacillales and *S. aureus* in the Order Bacillales. Analysis of both Orders using the KEGG database showed that the individual members of both Orders encode between 2 and 4 *fakB* genes.

FA selectivity of SpFakBs in cells

An experimental system to evaluate the FA selectivities of FA-binding proteins was developed using *S. aureus* strain JLB31 (Δ*fakB1* Δ*fakB2*) that was unable to incorporate exogenous FA because it lacks FA-binding proteins but expresses the *Sa*FakA kinase domain protein. A series of plasmids were constructed that expressed the individual FakBs governed by the *sarA* promoter (Table 1). The series of JLB31 strains each harboring a plasmid expressing a particular FakB were grown to an A_{600} of 0.5 and then a mixture of [d_4]16:0, -18:1, and -18:2 (10 μM each) was added to the cultures. After a 30-min incubation, the extent of each FA incorporated into PG was determined by MS (Fig. 2*A*). The assay was validated using *Sa*FakBs of known FA specificity. The expression of *Sa*FakB1 resulted in robust incorporation of [d_4]16:0, whereas the incorporation of the unsaturated FA in the mixture was not detected. In the strain expressing *Sa*FakB2, 18:1 was the most highly incorporated FA, although lower amounts of both [d_4]16:0 and -18:2 were detected. Strain JLB31/pCS119 (empty vector) did not express a FakB and did not incorporate any exogenous FA.

S. pneumoniae FakBs were interrogated in the same manner. *Sp*FakB1 supported the incorporation of [d_4]16:0, but not 18:1 or 18:2 (Fig. 2*A*). Oleate (18:1) was the highest incorporated FA in the strain expressing *Sp*FakB2, and more 18:2 was incorporated in the strain expressing *Sp*FakB3 as compared with 18:1 ($p = 0.03$) or [d_4]16:0 ($p = 0.001$) (Fig. 2*A*). These data point to *Sp*FakB3 as a binding protein for polyunsaturated FA, and the substrate preferences of *Sp*FakB2 and *Sp*FakB3 were further examined using a mixture of 3 polyunsaturated FA (Fig. 2*B*). *Sp*FakB2 clearly preferred 18:1, whereas *Sp*FakB3 was less specific in this assay utilizing 18:1, 18:2, and 18:3 although more 18:2 was incorporated as compared with 18:1 ($p = 7.0 \times 10^{-4}$) or 18:3 ($p = 2.3 \times 10^{-6}$) (Fig. 2*B*). These data suggested that *Sp*FakB3 extends the range of environmental FA that can be incorporated by the FA kinase system to polyunsaturated FA.

Biochemical analysis of SpFakB selectivity

One potential caveat to the cellular FA selectivity experiment was that incorporation also depended on the action of PlsX and PlsY, which themselves may have acyl chain selectivity that would impact the results. Therefore, *Sp*FakA and the three *Sp*FakBs were expressed and purified to evaluate FA preferences *in vitro* (Fig. 3*A*). All four proteins expressed well and were >90% pure judged by gel electrophoresis. Next, the apparent K_m for each of the *Sp*FakBs was determined to establish the foundation for the biochemical competition assay (Fig. 3*B*). *Sp*FakB2 and *Sp*FakB3 had the same apparent K_m (0.4 ± 0.09 and 0.5 ± 0.08 μM), whereas the *Sp*FakB1 K_m was 2.1 μM ± 0.6.

We used a competition assay to evaluate the utilization of FA by the individual *Sp*FakBs (Fig. 4). This assay used a ^{14}C-labeled FA substrate that matched the preferred substrate for each *Sp*FakB: [^{14}C]16:0 for *Sp*FakB1; [^{14}C]18:1 for *Sp*FakB2; and [^{14}C]18:2 for *Sp*FakB3. Unlabeled FA competitors were 80 μM. If the added FA was a substrate for the FA kinase reaction, then the amount of labeled product is reduced. *Sp*FakB1 activity measured with [^{14}C]16:0 was robust, and an excess of cold 16:0 added to the reaction significantly diminished labeled [^{14}C]16:0-phos-

Table 1
Strains, plasmids, and primers

	Description	Source
Strains		
AH1263	*S. aureus* strain USA300–0114, Erm-sensitive	46
JLB31	*fakB1*::ΦΝΣ Δ*fakB2* of strain AH1263	1
Sa178RI	Derived from *S. aureus* strain RN4220	47
TIGR4	Wildtype encapsulated *S. pneumoniae*	www.tigr.org
JMG1	TIGR4 with *fakB3* replaced with Kan cassette	This study
Plasmids		
pG164	Isopropyl 1-thio-β-D-galactopyranoside-inducible vector	47
pCS119	pCM28SarAP1promoter	48
pPJ480	pCS119 vector with RBS site	This study
pET28a	Expression vector	Novagen
pET28SpA	His tag *Sp*FakA expression vector	This study
pET28SpB1	His tag *Sp*FakB1 expression vector	This study
pET28SpB2	His tag *Sp*FakB2 expression vector	This study
pET28SpB3	His tag *Sp*FakB3 expression vector	This study
p*Sa*B1	pCS119 expressing *Sa*FakB1	This study
p*Sa*B2	pCS119 expressing *Sa*FakB2	This study
p*Sp*B1	pPJ480 expressing *Sp*FakB1	This study
p*Sp*B2	pPJ480 expressing *Sp*FakB2	This study
p*Sp*B3	pPJ480 expressing *Sp*FakB3	This study
pDL278	*E. coli*, Gram-positive shuttle vector	49
p*Sp*FakB3	*Sp*FakB3 *S. pneumoniae* expression plasmid	This study
pABG5	*E. coli*, Gram-positive shuttle vector	34
Primers	**Sequence (5′ to 3′)**	
Primer 1	CTCAAGTGGTAAATGGGTCAA	
Primer 2	AAATGGTTCGCTGGGTTTATCAGAAATTCTCCATCTTTGTCA	
Primer 3	GATAAACCCAGCGAACCATTT	
Primer 4	ATACAAATTCCTCGTAGGCGC	
Primer 5	GCGCCTACGAGGAATTTGTATTTGCATTCTTGACAAGAGGTG	
Primer 6	ATCATAATGCAGACTTCCCGC	
Primer 7	TGGAGAATTTCTATGACTTGG	
Primer 8	ATGCAATTAATCAATTTC	
pABGB3BamH1	CTTGGATCCATTTTCTCTCCTCTCAAA	
pABGB3Sac1	GATGAGCTCTTAATCAATTTCATAGCC	

phate formation. When an excess of either 18:1 or 18:2 was added, there was no change in the utilization of [^{14}C]16:0 indicating that these FA are poor substrates for *Sp*FakB1 (Fig. 4*A*). The activity of *Sp*FakB2 measured with [^{14}C]18:1 was effectively competed with 18:1, but not with 16:0 (Fig. 4*B*). The addition of 18:2 decreased the conversion of [^{14}C]18:1-phosphate indicating that 18:2 exchanged onto *Sp*FakB2, but the amount of [^{14}C]18:1-phosphate was not significantly different from the control (Fig. 4*B*). FA kinase activity with *Sp*FakB3 using [^{14}C]18:2 as a substrate was not decreased by 16:0. Both 18:1 and 18:2 were effective competitors but statistically more [^{14}C]18:2-phosphate remained when cold 18:1 was used as compared with when cold 18:2 was used ($p = 0.002$) meaning that 18:2 was a better substrate for *Sp*FakB3 (Fig. 4*C*). The range of FA competitors was extended to other polyunsaturated FA (18:3 and 20:4) (Fig. 4*D*). These experiments showed that *Sp*FakB3 utilized a broad spectrum of unsaturated FA but showed a statistically significant preference for 18:2 over 18:1 ($p = 0.02$), 18:3 ($p = 0.01$), or 20:4 ($p = 2.7 \times 10^{-4}$) (Fig. 4*D*).

FA utilization in a ΔfakB3 mutant

The physiological role of *fakB3* in *S. pneumoniae* FA uptake was evaluated by constructing a Δ*fakB3* knockout strain. Strain JMG1 (Δ*fakB3*) was constructed from strain TIGR4 by allelic replacement with a cassette encoding kanamycin resistance (Fig. 5*A*). PCR analysis showed the presence of the knockout allele and the absence of the *fakB3* gene in strain JMG1. The PG molecular species of strain JMG1 (Δ*fakB3*) was indistinguishable from TIGR4 (WT) when grown in C+Y (Figs. 1*A* and 5*B*) but TIGR4 incorporated more 18:2 than strain JMG1 (Δ*fakB3*) when grown in human serum (Figs. 1*C* and 5*C*). The incorporation of 18:2 was restored to WT levels in the complemented strain JMG1/p*Sp*FakB3 (Fig. 5*D*). These data validate a role for *Sp*FakB3 in the utilization of exogenous 18:2 for membrane lipid synthesis in *S. pneumoniae*.

Crystal structures of SpFakBs

The basis for the FA preferences of the *Sp*FakB proteins was revealed by the crystal structures of the three *S. pneumoniae* FA-binding proteins in complex with their respective FA ligands (Table 2). The *Sp*FakBs all have a two-domain protein-fold very similar to the other FakB protein family members that have been described (5, 12, 16, 17) (Fig. 6). The N-terminal domain consists of an EDD-fold fused to a 3-stranded antiparallel β-sheet and one α-helix. The carboxyl-terminal domain is a six-stranded β-sheet flanked by two α-helices on one side and three on the other. The surface arginine residue highlighted in Fig. 6 is conserved and required for high affinity binding to the FakA component of FA kinase (12). Its presence in all FakB structures explains why *Sp*FakBs function interchangeably with *Sa*FakA (Fig. 2*A*), and identifies the FakA-FakB binding locale. Furthermore, the overall surface charge distribution is similar in all three *Sp*FakBs (Fig. 6). The conservation of the FakB structure across isoforms and species accounts for their ability to interchangeably interact with their three protein partners: FakA, PlsX, and PlsY (5).

The SpFakB FA-binding tunnels

The unique distinguishing feature of the FakBs is the size and shape of the hydrophobic FA-binding tunnel located in the protein's interior that defines the FA binding selectivity. The

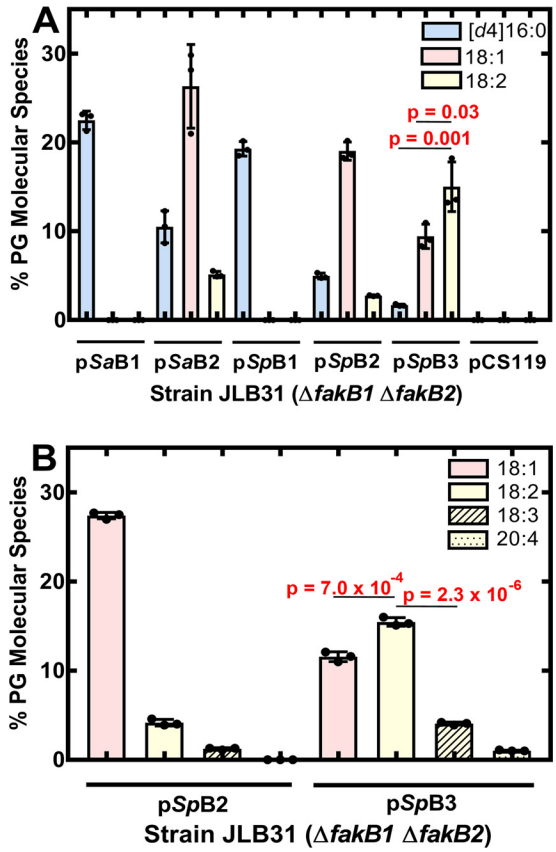

Figure 2. FA selectivity of *S. pneumoniae* FakB proteins *in vivo*. *S. aureus* strain JLB31 (Δ*fakB1* Δ*fakB2*) contains no functional *fakB* genes. Plasmids derived from pCS119 (control empty vector) were constructed to drive the expression of each of the *S. aureus* and *S. pneumoniae fakB* genes using the *sarA* promoter and were introduced into strain JLB31. *A*, the strain set was labeled with an equimolar mixture of [d_4]16:0, 18:1, and 18:2 (10 μM each) for 30 min and the contribution of each FA in the PG molecular species was determined by MS. *B*, strain JLB31 expressing *Sp*FakB2 or *Sp*FakB3 was labeled with an equimolar mixture of 18:1, 18:2, 18:3, and 20:4 (7.5 μM each) for 30 min, and the contribution of each unsaturated FA to the PG molecular species was determined by MS. Triplicate biological replicates were obtained, the areas under each peak in the spectra were summed and reported as a percent of the total area, and mean ± S.D. was plotted. Peaks containing elongation products, like 20:1 derived from 18:1, were included in the calculation for the contribution of the parent FA. Data are the mean ± S.D. of 3 individual data sets. Statistical differences between the FA incorporated in each strain was determined using Student's *t* test.

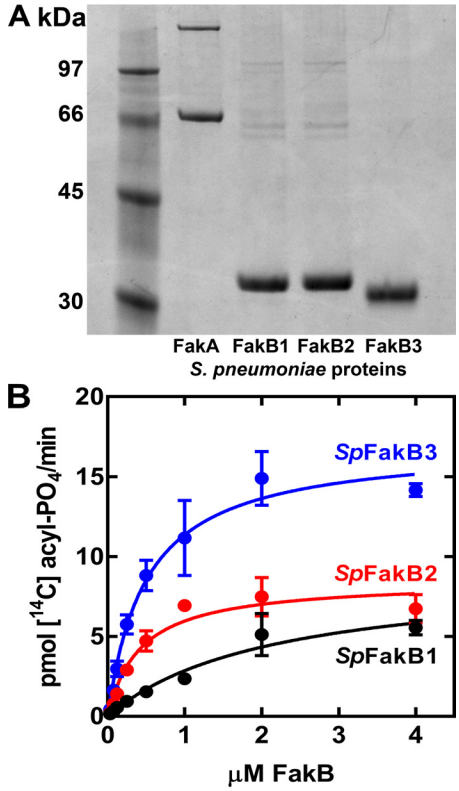

Figure 3. Biochemical validation and analysis of *S. pneumoniae* FakB proteins. *A*, purity of *Sp*FakA and the three FakB proteins assessed by gel electrophoresis and Coomassie-staining. *B*, dependence of FA kinase activity on FakB concentration in the biochemical assays using 20 μM [^{14}C]FA (*Sp*FakB1, [^{14}C]16:0; *Sp*FakB2, [^{14}C]18:1; and *Sp*FakB3, [^{14}C]18:2) and 0.2 μM *Sp*FakA.

*Sp*FakB1(16:0) and *Sa*FakB1(16:0) complexes are structurally very similar (Fig. 7*A*), and there is an overall root mean square deviation of 1.45 Å between the two aligned structures. The gently curved shapes of the two FA-binding pockets and the residues used to construct the pocket are similar in the two proteins, and in both cases, the FA carboxyl is fixed by a hydrogen bond network at the mouth of the tunnel. However, a notable difference in *Sp*FakB1 is a kink in the FA chain at carbon-2 that is not present in *Sa*FakB1, which displaces the acyl chains by 1.2 Å at this position. The equivalent residues *Sp*Ile28–*Sa*Leu28 and *Sp*Val264–*Sa*Val266 are displaced by 1.6 and 1.7 Å, respectively, to accommodate this kink at carbon-2 in the *Sp*FakB1(16:0) structure. The kink generates additional changes in the conformation of the FA in *Sp*FakB1(16:0) compared with *Sa*FakB1(16:0), and these are accommodated by other displacements between aligned equivalent residues in the tunnels: *Sa*Gly277–*Sp*Gly277, 0.9 Å; *Sa*Ile124–*Sp*Pro123, 0.7 Å; *Sa*Leu120–*Sp*Ile119, 1.2 Å; and *Sa*Ala158–*Sp*Ala157, 0.6 Å.

The *Sp*FakB2(18:1Δ9) structure is also very similar to the *Sa*FakB2(18:1Δ9) structure (Fig. 7*B*) with an overall root mean square deviation of 1.27 Å between the two aligned structures. Despite the low level of sequence identity between the two proteins (29%), the amino acids that create their FA tunnels both generate the same distinctive kinked cavities that are required to accommodate the *cis* double bond in the middle of the acyl chain. Similar to FakB1, the FA carboxyl is fixed by a hydrogen bond network at the entrance of the tunnel that comprises highly conserved and closely aligned residues in *Sp*FakB2 and *Sa*FakB2; *Sp*Leu29–*Sa*Leu23 (0.2 Å), *Sp*Ser94–*Sa*Ser93 (0.3 Å), *Sp*Arg171–*Sa*Arg170 (0.4 Å), and *Sp*His265–*Sa*His266 (0.5 Å). The bound 18:1 adopts very similar conformations in *Sp*FakB2 and *Sa*FakB2 but begins to diverge at carbon-13 and is separated by 0.5 Å at the terminal methyl. Accordingly, equivalent residues that surround the distal end of the FA are more displaced than those at the proximal end: *Sp*Ser230–*Sa*Ala230, 1.0 Å; *Sp*Trp271–*Sa*Ile272, 0.5 Å; *Sp*Ala272–*Sa*Gly273, 1.3 Å.

The *Sp*FakB3(18:2(Δ9Δ12)) complex structure reveals a distinctive gourd-like FA-binding pocket that highlights how the interiors of these proteins have evolved to perfectly accommodate FA of different structures (Fig. 8*A*). Like FakB1 and FakB2, the proximal end of the FakB3 tunnel is relatively narrow and straight to accommodate the first 7 carbons of the acyl chain. However, at this point, the tunnel expands into a wide cavern

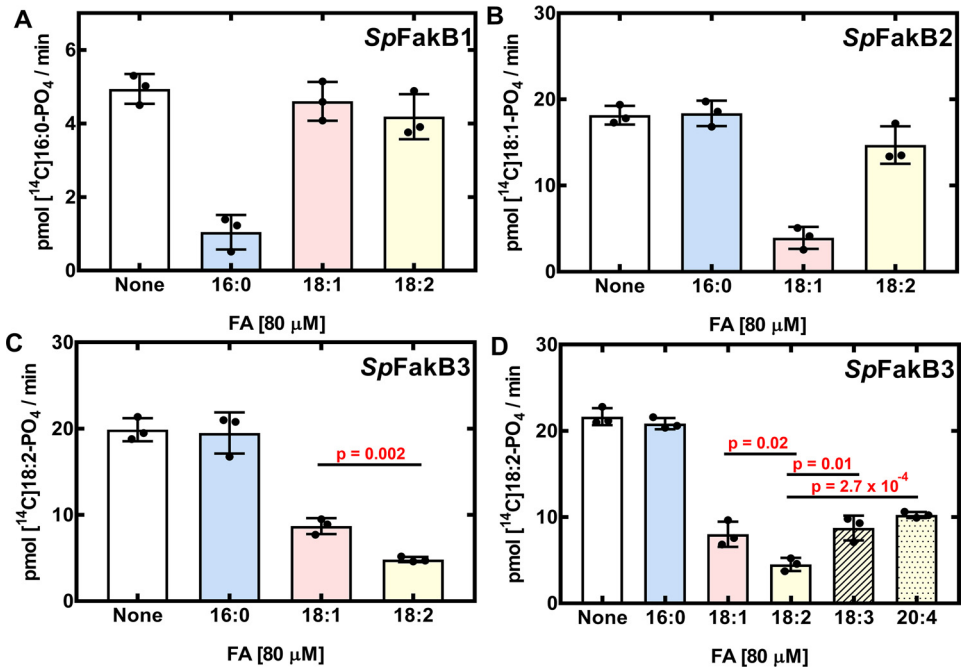

Figure 4. Analysis of FakB selectivity *in vitro*. FA kinase assays were used to investigate the selectivites of the *Sp*FakBs. Each *Sp*FakB was assayed in the presence of 0.2 μM *Sp*FakA using 20 μM of an individual radiolabeled FA that corresponds to its substrate preference. [^{14}C]16:0 was the substrate for *Sp*FakB1, [^{14}C]18:1 was the substrate with *Sp*FakB2, and [^{14}C]18:2 was the substrate for *Sp*FakB3. Then to each assay 80 μM cold FA competitor was added. *A*, *Sp*FakB1. *B*, *Sp*FakB2. *C*, *Sp*FakB3, and *D*, *Sp*FakB3. Experiments were performed in triplicate. Data are the mean ± S.D. of 3 individual data sets. Statistical differences between the FA incorporated in each strain was determined using Student's *t* test.

that allows FA with multiple *cis* double bonds to curl up inside the protein. The volume of the tunnel is 110.4 Å^3, which is larger than the linear FakB1 tunnel (67.5 Å^3) and slightly larger than the kinked FakB2 tunnel (102 Å^3). Another distinguishing feature of *Sp*FakB3 compared with FakB1 and FakB2 is that it uses a different hydrogen bond network to lock the FA carboxyl in place (Fig. 8*B*). The typical FakB configuration places Ser on one carbonyl oxygen and a His-Thr dyad on the other side to form a Ser-FA carbonyl-Thr-His network (12). In contrast, in *Sp*FakB3, a tyrosine (Tyr-268) plays the role of histidine and a serine (Ser-63) replaces threonine to form a Ser-FA carbonyl-Ser-Tyr network. There are also two structured water molecules in *Sp*FakB3 hydrogen bonded to the FA carbonyl that mediate hydrogen bond connections between the FA carbonyl and Arg-173, Gly-92, and Ser-63. Arg-173 also forms a hydrogen bond with Tyr-268 and a water-mediated connection with Asn-171.

Further insights into the SpFakB1 and SpFakB2 tunnel specificities

In *Sp*FakB1(16:0), the terminal methyl of the 16:0 chain is packed against the protein at the end of the pocket suggesting that the bend at carbon-2 may be required for the 16:0 chain to fit into the pocket. This idea was tested by determining the structure of *Sp*FakB1 in complex with the shorter 14:0 FA with the prediction that the carbon-2 bend would not be present. An overlay of the *Sp*FakB1(16:0) and *Sp*FakB1(14:0) structures shows that the two FA overlay along the entire length of the binding tunnel and that the bend at carbon-2 is also present in the 14:0 structure (Fig. 9*A*). *Sa*Ile232 acts as a swinging gate to increase or decrease the tunnel length in *Sa*FakB1, but residue *Sp*Ile232 did not change orientation or position in the *Sp*FakB1 structures loaded with either 16:0 or 14:0. In the *Sp*FakB1(16:0) structure, the terminal FA methyl carbon is 3.7 Å away from *Sp*Ile232. There were small changes in Phe-192 side chain that slightly close the end of the tunnel in the *Sp*FakB1(14:0) structure, but otherwise the two structures are almost identical except for the length of the acyl chain. Thus, the carbon-2 bend is an integral feature of the *Sp*FakB1 FA complex.

Another question is how the substrate selectivity of *Sp*FakB2 is related to its biological function(s). *S. aureus* does not produce unsaturated FA and thus *Sa*FakB2 does not have a specific role in lipid homeostasis in the organism (5). However, *S. pneumoniae* does produce monounsaturated FA suggesting that *Sp*FakB2 may have a role in lipid metabolism in this organism. *S. pneumoniae de novo* biosynthesis produces 18:1, although the primary location of the double bond is at carbon-11 instead of carbon-9 as found in mammals (6). The flexibility of *Sp*FakB2 to bind these two monounsaturated FA was investigated by determining the structure of the *Sp*FakB2(18:1Δ11) complex and comparing it to the structure of *Sp*FakB2(18:1Δ9) (Fig. 9*B*). The binding pocket has enough space between the 9 and 12 carbons to accommodate either of the sp^2-hybridized double bonds. The overlay of these two structures shows that they are essentially identical with regard to the size and shape of the FA-binding tunnel and the positioning of the residues that form the binding pocket. The different locations of the sp^2 double bond conformations are clearly seen in the electron density map, and the maximum divergence of the two acyl chains is only 0.7 Å in the immediate area between the locations of the double bonds. These data illustrate that *Sp*FakB2 participates in the activation of both endogenous *cis*-vaccinate and exogenous oleate derived from the host.

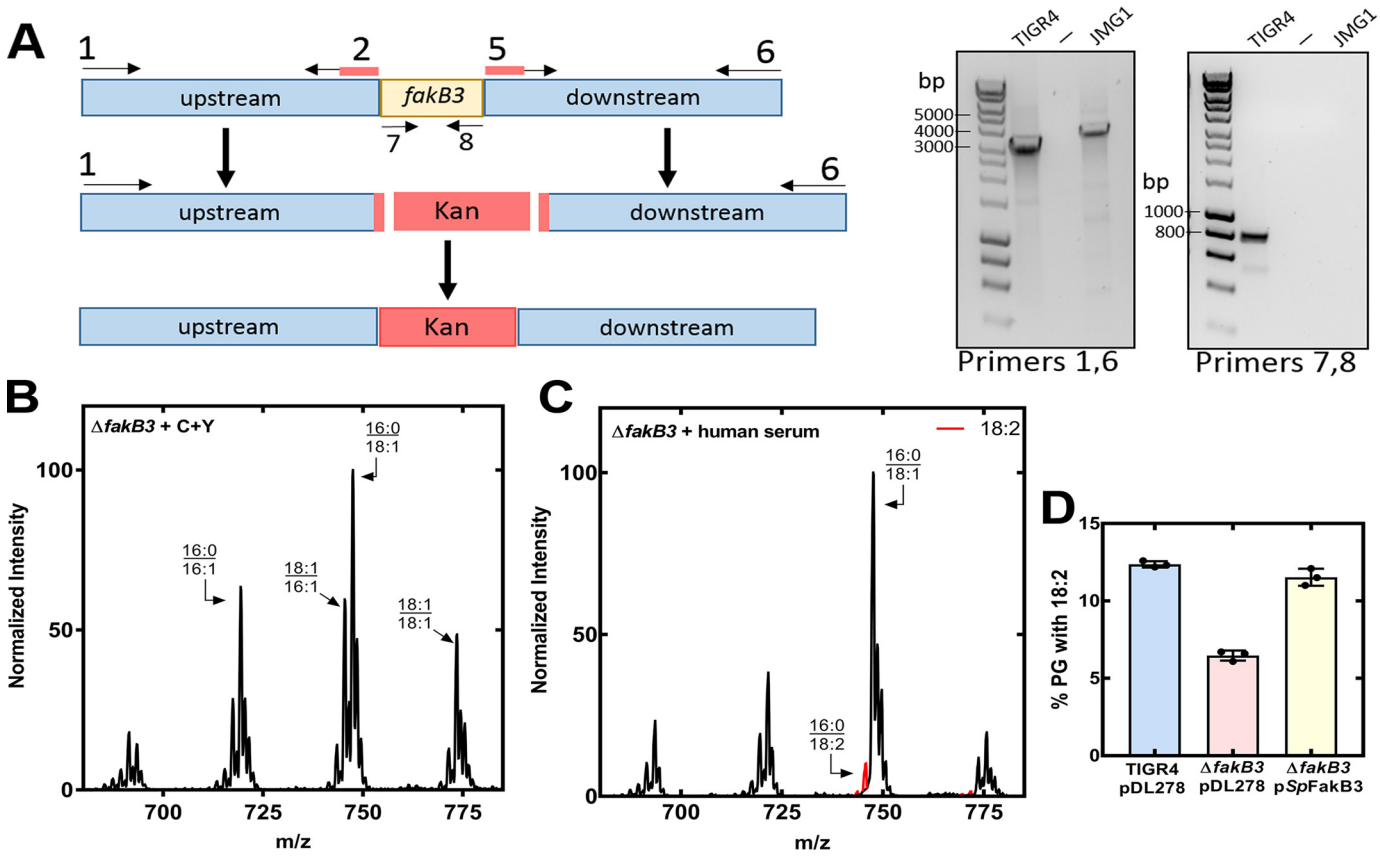

Figure 5. FA acquisition in a *S. pneumoniae* Δ*fakB3* deletion strain. *A*, schematic diagram illustrating the construction of strain JMG1 (Δ*fakB3*). The final construct has the *fakB3* gene replaced with a cassette expressing kanamycin resistance. Primers 1 and 6 showed the exchange of the *fakB3* gene for the kanamycin cassette, and primers 7 and 8 confirmed that *fakB3* was absent from the genome. Construction details are provided under "Experimental procedures" and primer sequences are listed in Table 1. *B*, representative spectra of *S. pneumoniae* strain JMG1 (Δ*fakB3*) grown in C+Y media (*C*) and grown in 50% human serum, 50% C+Y medium human serum. *D*, TIGR4, JMG1 (Δ*fakB3*), and JMG1/p*Sp*FakB3 were grown in 50% human serum, 50% C+Y medium, PG mass spectra from triplicate biological replicates were obtained, the areas under each peak in the spectra were summed, the molecular species containing 18:2 as a percent of the total area were calculated, and the mean ± S.D. was plotted.

Discussion

The biochemical and structural data lead to a model for FA metabolism in *S. pneumoniae* outlined in Fig. 10. The biosynthetic pathway in the absence of exogenous FA proceeds via the FASII collection of enzymes to long-chain acyl-ACP (18), which is then distributed to PlsY (via PlsX) or PlsC to produce phosphatidic acid, the precursor to all membrane glycerophospholipids (19). In the presence of exogenous FA, transcription of the FASII genes is potently suppressed by binding of the FabT–acyl-ACP repressor complex to promoters within the FASII gene cluster (6, 10). The repression of FASII gene expression by exogenous FA is mediated by acyl-ACP2 (9) (the *acpP2* gene that is in an operon with *plsX*). This regulatory loop shuts off *de novo* FA synthesis, and only exogenous FA are used for phospholipid synthesis (3). These exogenous FA are not significantly elongated even though they are converted to acyl-ACP because the FASII elongation system is suppressed. The three FakBs of *S. pneumoniae* characterized in this study participate in this FA sensing pathway by providing a mechanism to activate a spectrum of saturated, monounsaturated, and polyunsaturated FA found at the infection site for FA∼P and acyl-ACP formation. *Sp*FakB1 has the most restricted FA binding preference and effectively excludes unsaturated FA with kinked acyl chains due to the straight shape of its FA-binding tunnel. *Sp*FakB2 prefers monounsaturated FA. *Sp*FakB2 has a kinked FA-binding tunnel that accommodates both 18:1Δ11, the monounsaturated fatty acid produced by *S. pneumoniae*, and 18:1Δ9, a prevalent mammalian FA. Although *Sp*FakB2 prefers to bind monounsaturated FA, it does not exclude saturated FA, which are flexible and capable of fitting into the kinked binding pocket. *Sp*FakB2 also has a weak capacity to bind 18:2. *Sp*FakB3 has a wider FA-binding pocket that allows the binding of polyunsaturated FA, like 18:2, with multiple *cis* double bonds. The gourd-shaped pocket within *Sp*FakB3 means that it can present a variety of FA structures to FakA. The multiple FakBs of the FA kinase activation system coupled with the repression of *de novo* synthesis means that *S. pneumoniae* can efficiently and exclusively utilize the entire spectrum of mammalian FA found at the infection site for phosphatidic acid synthesis (Fig. 10).

*Sp*FakB3 is differentiated from most FakBs by having a different hydrogen bond network that interacts with the FA carboxyl group (Fig. 9*B*). The majority of bacterial FA-binding proteins use a Ser-FA carboxyl-Thr-His hydrogen bond network to fix the FA carboxyl at the entrance of the FakB FA-binding tunnel (12), but in about 5% of the FakB sequences, a tyrosine is substituted at the position of the histidine residue. *Sp*FakB3 is one of the FA-binding proteins with a Ser-FA carboxyl-Ser-Tyr hydrogen bond network. Disruption of this hydrogen bond net-

Table 2
Data collection statistics for *Sp*FakB fatty acid complexes

Protein	*Sp*FakB1	*Sp*FakB1	*Sp*FakB2	*Sp*FakB2	*Sp*FakB3
Fatty acid	Myristate (14:0)	Palmitate (16:0)	Oleate (18:1Δ9)	Vaccinate (18:1Δ11)	Linoleate (18:2Δ9,12)
PDB ID	**6NOK**	**6DKE**	**6DJ6**	**6NR1**	**6CNG**
Precipitant	PEG2/D7	PEG2/D7	Classics suite/A5	LMB/D12	JCSG+/B7
Cryoprotectant	Paraffin/paratone-N (1:1)	25% Glycerol	25% Glycerol	25% Glycerol	25% Glycerol
Data collection					
Beamline	SER-CAT 22-BM	SER-CAT 22-ID	SER-CAT 22-ID	SER-CAT 22-BM	SER-CAT 22-ID
Detector	MarCCD 300HS	Dectris Eiger X 16 M	Dectris Eiger X 16 M	MarCCD 300HS	MarCCD 300HS
Temperature (K)	100	100	100	100	100
Wavelength (Å)	1.0000	1.0000	1.0000	1.0000	1.0000
Space group	P21	P21	P212121	P212121	P21
Unit cell parameters (Å)					
a, *b*, *c*	37.56,66.32,46.95	46.83,62.34,50.43	59.72,103.85,108.17	59.65,103.41,107.93	52.78,103.41,67.47
α, β, γ	90.00,95.75,90.00	90.00,95.94,90.00	90.00,90.00,90.00	90.00,90.00,90.00	90.00,112.99,90.00
Resolution range (Å)	66.32–1.69	62.34–1.76	74.92–1.90	74.67–2.10	62.11–1.47
R_{merge}	0.056 (0.669)[a]	0.059 (0.497)	0.109 (0.827)	0.101 (0.616)	0.036 (0.544)
$R_{r.i.m.}$ or R_{meas}	0.066 (0.790)	0.072 (0.613)	0.129 (0.978)	0.113 (0.693)	0.044 (0.669)
$R_{p.i.m.}$	0.34 (0.415)	0.042 (0.355)	0.067 (0.510)	0.050 (0.311)	0.025 (0.386)
Number observations	93,246 (4,636)	76,979 (4,403)	197,121 (12,541)	190,517 (15,213)	323,223 (15,293)
Number unique reflections	25,680 (1,310)	28,063 (1,592)	52,631 (3,366)	39,625 (3,194)	108,472 (5,188)
Multiplicity	3.6 (3.5)	2.7 (2.8)	3.7 (3.7)	4.8 (4.8)	3.0 (2.9)
Mn $I/\sigma(I)$	16.2 (2.0)	10.6 (2.0)	9.4 (1.9)	9.0 (2.0)	15.0 (2.0)
Mn(I) half-set corr.	0.998 (0.667)	0.995 (0.746)	0.993 (0.479)	0.998 (0.799)	0.999 (0.574)
Completeness (%)	99.8 (99.8)	97.9 (98.7)	98.3 (99.6)	99.7 (99.7)	96.2 (94.1)
Wilson B-factor (Å^{-2})	17.3	22.0	17.03	21.7	17.3
Model quality					
Twinning (operator, %)	NA[b]	NA	NA	NA	*-h,-k,h+l*, 49.8
Monomers/asymetric unit	1	1	2	2	2
R_{work}/R_{free} value (%)	15.2/20.0	17.0/20.6	17.1/22.7	18.4/24.1	13.7/16.5
R.m.s. deviations					
Bonds (Å)	0.017	0.005	0.010	0.009	0.014
Angles (°)	1.482	0.751	1.361	0.915	1.134
Coordinates error (ML, Å)[c]	0.17	0.22	0.12	0.24	n/a
Protein residues	285	283	555	557	562
Average B factor (Å^2)					
All atoms	25.1	29.9	25.4	36.5	21.2
Protein atoms	23.4	28.4	23.8	36.4	19.1
Fatty acid atoms	17.5	19.8	31.2	33.9	30.3
Solvent atoms	38.9	41.9	37.7	37.8	30.6
Ramachandran plot					
Favored (%)	96.8	98.2	98.5	98.6	96.0
Allowed (%)	2.5	1.8	1.3	1.5	3.8
Outliers (%)	0.7	0	0.2	0.8	0.2
Clashscore	2.8	2.2	2.3	4.3	8.6

[a] Values in parentheses are for the highest resolution shell. $R_{merge} = \Sigma(I-\langle I\rangle)/\Sigma(I)$; where I is the intensity measured for a given reflection, $\langle I\rangle$ is the average intensity for multiple measurements of this reflection. $R_{p.i.m.} = (\Sigma[1/(n-1)]\text{^}1/2.\ \Sigma|I-\langle I\rangle|)/\Sigma(I)$. $R_{work} = \Sigma||F_{obs}| - |F_{calc}||/\Sigma|F_{obs}|$; where F_{obs} and F_{calc} are the observed and calculated structure factor amplitudes, respectively. R_{free} is R_{work} for the 5% excluded reflections during refinement.
[b] NA, not applicable.
[c] ML is maximum likelihood.

work by mutagenesis shows that it is critical to the stability of the FA-binding protein. For example, the *Sa*FakB2(S93A) mutant severs the connection to one side of the FA carbonyl and results in a 17 °C decrease in the denaturation temperature of the protein (12). Whether the hydrogen bond network is associated with polyunsaturated FA binding or has some other mechanistic significance is unclear.

The bacterial FA-binding proteins are very different from their mammalian counterparts (20, 21). The mammalian proteins are about half the size of the bacterial proteins and have a β-barrel structure consisting of 10 antiparallel β-sheets with 2 α-helices between the first and second β-strands (22–24). The carboxyl group of the FA is oriented inward and electrostatically bound to Arg-106 in the intestinal FA-binding protein (25), whereas the FA carboxyl in the bacterial binding proteins is exposed as the phosphorylation site in the FakB(FA) complexes. Another key difference is that the mammalian FA-binding proteins lack acyl chain selectivity (20, 21, 26) and have large cavities (PDB ID 4TJZ = 245 Å^3; PDB ID 5CE4, 291 Å^3; calculated using CASTp (27)) that in some cases bind two FAs (20, 22). The bacterial FA-binding proteins have smaller, narrow tunnels that impart substrate selectivity to these binding proteins. The expanded hydrophobic binding pocket of *Sp*FakB3 is most reminiscent of the large, nonselective hydrophobic pockets that occur in mammalian FA-binding proteins, although the 110 Å^3 volume of *Sp*FakB3 is half the size of the larger mammalian pockets. Mammalian FA-binding proteins are isolated in both their ligand-free and FA-bound forms, and there is no clear relationship between FA binding and protein stability (28). The FA-free FakBs are not stable and only FA-bound FakBs have been purified (5, 12). Mutations in the hydrogen bond network that fixes the FA carboxyl significantly destabilize *Sa*FakB2 (12). The mammalian FA-binding proteins pick up and deposit FA into phospholipid bilayers, and the 2-helix motif is thought to act as the entry and exit flap for the FA (22–24, 29, 30). The bacterial FA-binding proteins also exchange FA with FA in phospholipid bilayers (1) and transfer the phosphorylated FA to two enzyme partners, PlsX and PlsY (5). The protein movements in FakB that allow the entry and exit of the FA and acyl-phosphate remain to be defined.

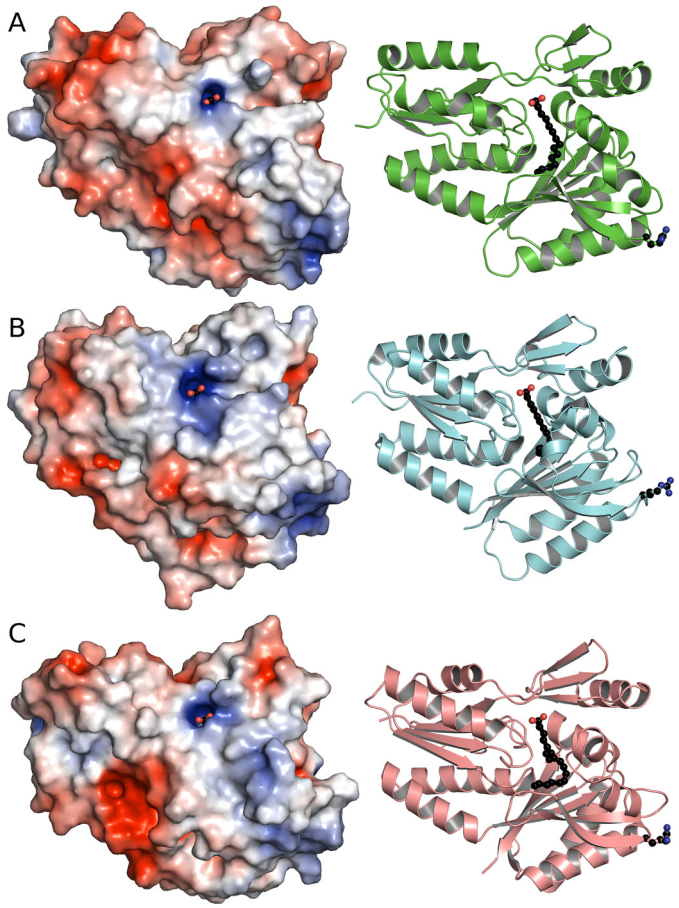

Figure 6. The overall structures of the three *Sp*FakBs. The structures of the 3 *Sp*FakBs were determined and are shown in ribbon diagram adjacent to the surface rendering. The surface Arg residue that is critical for FakA binding is located at the *bottom right* of each molecule and are shown as balls and sticks in the ribbon diagrams. The surface potential of each *Sp*FakB show similar patterns of charge distribution. *A*, *Sp*FakB1. *B*, *Sp*FakB2. *C*, *Sp*FakB3. The ribbon structures were rendered with PyMOL and the surface potentials were calculated with APBS in PyMOL.

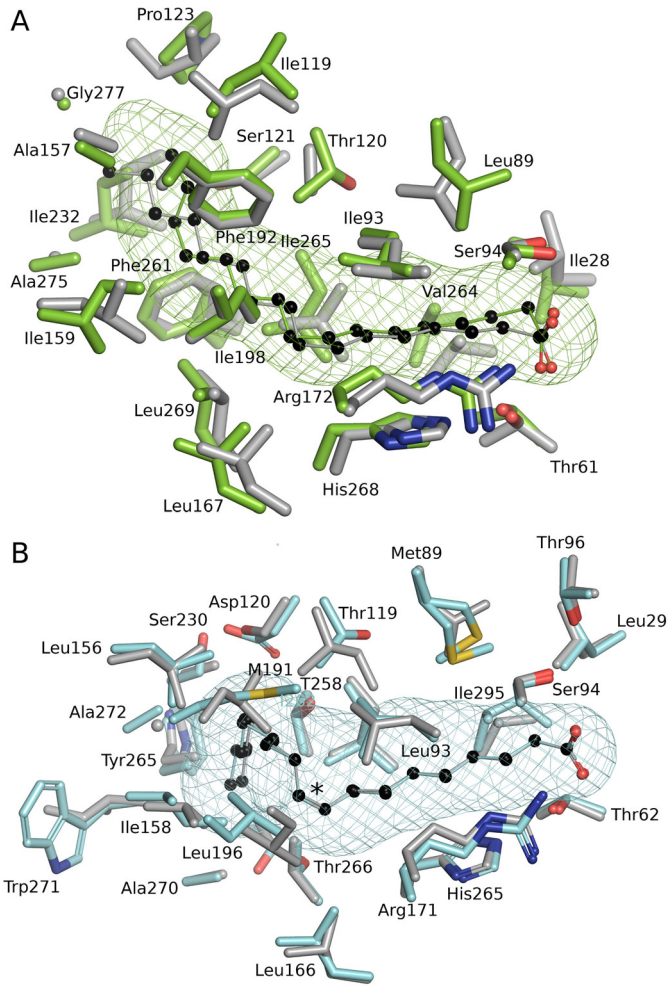

Figure 7. Conservation of the FA-binding pocket shapes in saturated and monounsaturated FA-binding proteins of *S. pneumoniae* and *S. aureus*. *A*, structural alignment of *Sp*FakB1(16:0) (*green*, PDB ID, 6DKE) and *Sa*FakB1(16:0) (*gray*, PDB ID, 5UTO) FA-binding tunnels and surrounding residues as aligned with PyMOL. *B*, *Sp*FakB2(18:1Δ9) (*cyan*, PDB ID 6DJ6) and *Sa*FakB2(18:1Δ9) (*gray*, PDB ID, 4X9X). The coordinate alignment was based on the aligned tunnel residues in PyMOL. *Asterisk* indicates sp^2 hybridization of the double bond. The bound FA are depicted as colored *sticks with black carbon spheres*. The *meshes* that delineate the hydrophobic cavity within the proteins were computed with CAVER/PyMOL.

Experimental procedures

Materials

Sources of supplies were: PerkinElmer Life Sciences, [^{14}C]16:0 (specific activity, 56.1 mCi/mol), [^{14}C]18:1 (specific activity, 59 mCi/mol), [^{14}C]18:2 (specific activity, 54.5 mCi/mol); Millipore-Sigma, all FA and human serum (lot number SLBX0350); Cambridge Isotope Laboratories, Inc., 7,7,8,8-tetradeuteriohexadcanoic acid ([d_4]16:0); Sigma, all reagents for buffers; New England Biolabs (Ipswich, MA), restriction enzymes; Invitrogen, Anza alkaline phosphatase, T4 DNA ligase master mix, and DNA blunt end kit for blunt end ligation. Proteins were expressed, purified, and FA exchange was accomplished as described (1, 5, 12).

Bacterial strains

DNA sequences were synthesized for each of the *S. aureus* and *S. pneumoniae* FakB genes (Invitrogen). The DNA sequences for *S. aureus fakB1* (SaUSA300_0733) and *fakB2* (SaUSA300_1318) included a ribosomal binding site and a His_6 tag on the N terminus. Each *S. aureus fakB* sequence was cloned into plasmid pCS119, which has a pCM28 backbone (31), no ribosomal binding site, and uses a *sarA* P1 promoter to drive expression. DNA sequences for *S. pneumoniae* strain TIGR4 *fakB1* (SP_1557), *fakB2* (SP_1112), and *fakB3* (SP_0742) genes did not contain a ribosomal binding site or a His_6 tag and were cloned into pET28a (Novagen), to add an N-terminal His_6 tag, and ligated into pPJ480 (32), which is a pCS119 plasmid derivative containing the *sarA* P1 promoter as well as a ribosomal binding site. Restriction followed by ligation reactions were used to insert the *fakB* gene of interest into either pCS119 (*S. aureus* expression) or pPJ480 (*S. pneumoniae* expression). The ligation mixture was transformed into Top10 *Escherichia coli*-competent cells (Invitrogen) and selected on Luria broth with carbenicillin (100 μg/ml). Purified plasmids were passaged through strain Sa178R1 to acquire the *S. aureus* DNA methylation pattern, re-isolated, and electroporated into strain JLB31.

Strain JMG1 (Δ*fakB3*) was constructed by gene splicing by overlap extension PCR, which allowed for the creation of a gene deletion with a kanamycin resistance cassette in its

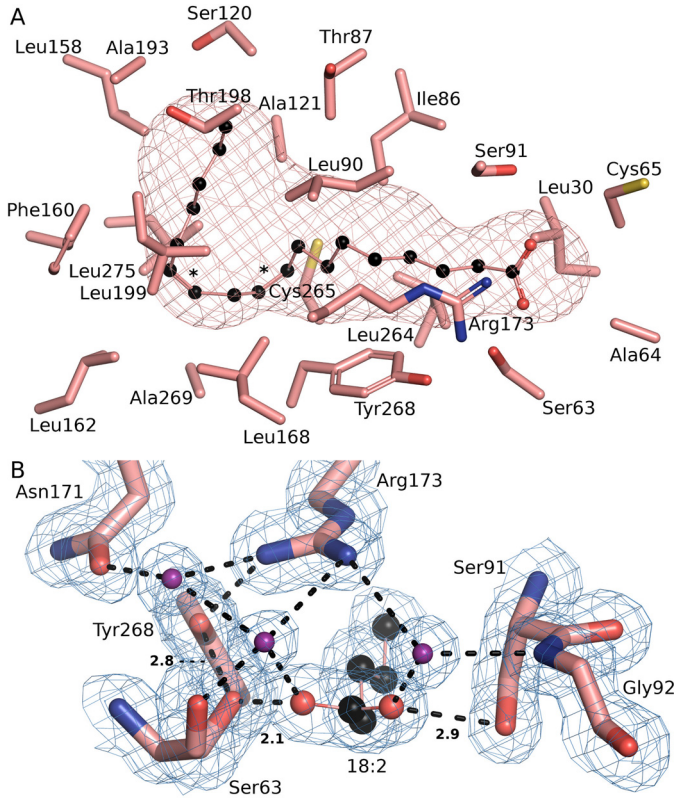

Figure 8. Unique aspects of the *Sp*FakB3 structure. *A*, view of the *Sp*FakB3 FA-binding tunnel and associated residues as visualized using CAVER to outline the interior volume of FakB3(18:2(Δ9Δ12)) (PDB ID 6CNG) (*salmon*). FA carbons are *black*. *B*, the *Sp*FakB3 Ser-91–FA–Ser-63–Tyr-268 hydrogen bond network that fixes the position of the FA carbonyl in the protein. FA carbons are *black*, FA and amino acid oxygens are *red*, and water molecules are colored *purple*. The *blue mesh* represents the experimental electron density contoured at 1 σ. *Dashed lines* indicate hydrogen bonds and the lengths in Å of the three key interactions are shown.

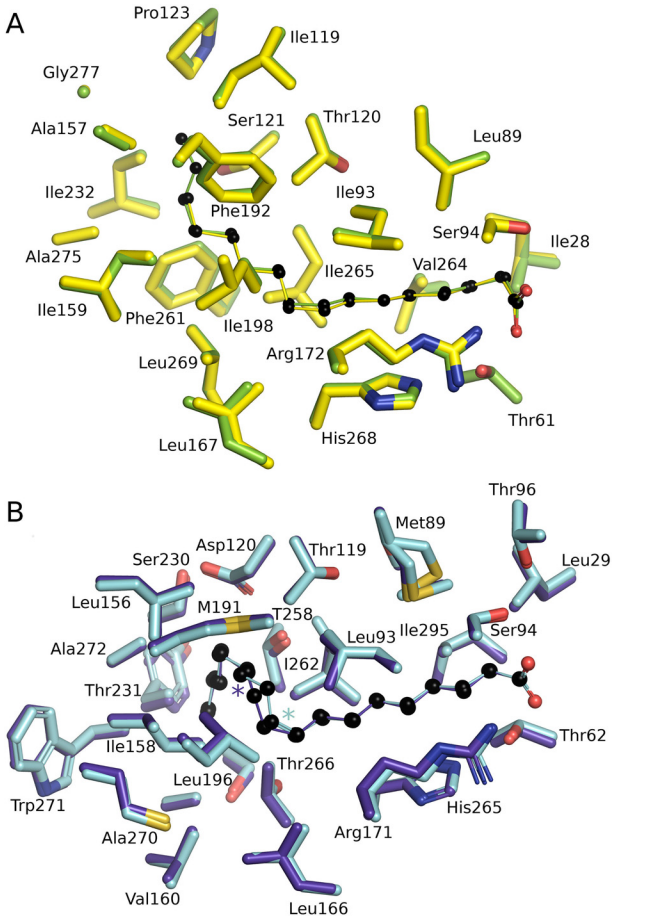

Figure 9. Versatility of FA binding by *Sp*FakB1 and *Sp*FakB2. *A*, structural alignment of *Sp*FakB1(14:0) (*yellow*, PDB ID 6NOK) and *Sp*FakB1(16:0) (*green*, PDB ID 6DKE). The fatty acids are presented as colored sticks with carbon spheres in *black*. *B*, structural alignment of *Sp*FakB2 with C18:1Δ9, (*cyan*, PDB ID 6DJ6) and *Sp*FakB2 with C18:1Δ11 (*purple blue*, PDB ID, 6NR1). *Colored asterisks* indicate locations of the sp^2 hybridized double bonds. The coordinate alignments were based on the FA using MCSALIGN plugin for PyMOL.

place (33). Briefly, primers 1 and 2 were used to amplify the upstream region (~1 kb) and primers 5 and 6 were used to amplify the downstream region (~1 kb) of the *fakB3* (locus tag, SP_0742) gene from TIGR4 genomic DNA (Fig. 5*A*; Table 1). Primers 3 and 4 were used to amplify the kanamycin cassette (~1.5 kb) from the pABG5 plasmid. These three PCR products underwent another PCR amplification using primers 1 and 6 to generate a linearized hybrid construct with the *fakB3* gene replaced by the kanamycin cassette (Fig. 5*A*). The linear DNA was run on an agarose gel and purified before being transformed. To transform 1 ml of TIGR4 culture in C+Y media (A_{600} = 0.07), 3 μl of competence pheromone were incubated at 37 °C for 13 min before 5 μl of the linearized DNA was added and incubated at 37 °C for 4 h. Cells were plated on 3% blood agar plates with kanamycin (400 μg/ml) and neomycin (20 μg/ml) and incubated overnight at 37 °C. The colonies that arose were purified and genomic DNA was extracted. PCR was used to confirm the deletion using primers 1 and 6 and 7 and 8 (Fig. 5*A*; Table 1).

The *Sp*FakB3 expression plasmid was made by engineering a gene sequence Genewiz) with an EcoRI site on the 5′ end followed by a ribosomal binding site taken from the pABG5 vector, a His_6 tag, the TIGR4 *S. pneumoniae fakB3* nucleotide sequence, and ClaI restriction site at the 3′ end of the gene. The assembled expression construct was inserted into pUC57. Purified plasmid was passaged through INV110 *E. coli*-competent cells as the ClaI site was sensitive to Dam methylation. The pUC57 containing the *fakB3* insert and pABG5 vector were cut using EcoRI and ClaI, ligated, and transformed into Top10 *E. coli*-competent cells. The resulting plasmid was purified and amplified using PCR with primers pABGB3BamHI and pABGB3SacI to amplify the *fakB3* insert as well as the upstream region of the pABG5 plasmid containing the *rofA* promoter (34). The pABGB3SacI primer changed the 3′ restriction site to SacI so that the resulting amplicon could be inserted into pDL278. A restriction digest was performed on the PCR product using BamHI and SacI and the product was run on an agarose gel before the band was extracted and purified. The *fakB3* fragment was inserted into linearized pDL278 via blunt end ligation and subsequently transformed into Top10 *E. coli*-competent cells. The resulting plasmid was purified and sequenced before being transformed into strain JMG1 (Δ*fakB3*) and plated on 3% blood agar plates with kanamycin (400 μg/ml), spectinomycin (150 μg/ml), and neomycin (20 μg/ml). TIGR4/pDL278 and JMG1/pDL278 were made using the above-mentioned

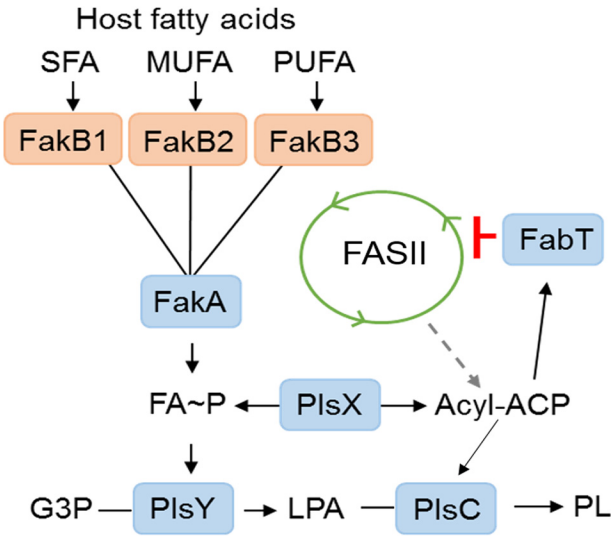

Figure 10. Model for the function of FakB proteins in *S. pneumoniae*. The *de novo* phospholipid biosynthetic pathway in *S. pneumoniae* delivers acyl-ACP generated by the FASII system to PlsX to provide FA∼P to the glycerol phosphate (*G3P*) acyltransferase (*PlsY*) to form lysophosphatidic acid (*LPA*) and initiate phospholipid synthesis. Acyl-ACP is also a substrate for PlsC that completes the formation of phosphatidic acid, the universal precursor to membrane glycerolipids (*PL*). At the infection site the host provides an environment containing a spectrum of saturated (*SFA*), monounsaturated (*MUFA*), and polyunsaturated (*PUFA*) FA. Each of these types of FA are the preferred ligand for binding to unique FakB-binding proteins that carry the FA to FakA, where they are phosphorylated. The resulting FA∼P is a substrate for PlsY or is converted to acyl-ACP by PlsX to act as substrate for PlsC. The long-chain acyl-ACP binds to the FabT transcriptional regulator, and the complex binds tightly to the promoters within the FASII gene cluster to potently suppresses the expression of the entire biosynthetic gene set and shut off acyl-ACP formation from FASII. The acyl-ACP may also enter FASII and be elongated, although this is a minor pathway due to the strong suppression of the elongation cycle enzymes by FabT–acyl-ACP complex.

transformation protocol and plated on the same plates used to select for strain JMG1.

FA incorporation experiments

S. aureus and *S. pneumoniae* strains AH1263 and TIGR4, respectively, were inoculated into 5 ml of growth medium (*S. aureus*, Luria broth; *S. pneumoniae*, C+Y) at an A_{600} of 0.05, and grown at 37 °C to an A_{600} of 0.5, harvested, and resuspended in 5 ml of 50% human serum/LB (*S. aureus*) or 50% human serum/C+Y (*S. pneumoniae*). Cultures were incubated 4 h before cells were harvested, washed twice in growth medium, and once in PBS, and lipids were extracted (35). Plasmids containing *S. pneumoniae* or *S. aureus* genes in strain JLB31 were grown in Luria broth at 37 °C to an A_{600} of 0.5. A FA mixture (10 μM each) of [d_4]16:0, -18:1, and -18:2, along with Brij-58 (0.1%) was added to the culture, incubated at 37 °C for 30 min, and the lipids were extracted. Protocol was the same for polyunsaturated FA incorporation with the exception that a mixture (7.5 μM each) of 18:1, 18:2, 18:3, and 20:4 was added to the growth medium.

Lipid extracts were resuspended in chloroform:methanol (1:1). PG was analyzed using a Shimadzu Prominence UFLC attached to a QTrap 4500 equipped with a Turbo V ion source (Sciex). Samples were injected onto an Acquity UPLC BEH HILIC, 1.7 μm, 2.1 × 150-mm column (Waters) at 45 °C with a flow rate of 0.2 ml/min. Solvent A was acetonitrile, and solvent B was 15 mM ammonium formate, pH 3. The HPLC program was the following: starting solvent mixture of 96% A/4% B, 0 to 2 min isocratic with 4% B; 2 to 20 min linear gradient to 80% B; 20 to 23 min isocratic with 80% B; 23 to 25 min linear gradient to 4% B; 25 to 30 min isocratic with 4% B. The QTrap 4500 was operated in the Q1 negative mode. The ion source parameters for Q1 were: ion spray voltage, −4500 V; curtain gas, 25 psi; temperature, 350 °C; ion source gas 1, 40 psi; ion source gas 2, 60 psi; and declustering potential, −40 V. The system was controlled by the Analyst® software (Sciex). The sum of the areas under each peak in the mass spectra was calculated and the percent of each molecular species present was calculated with LipidView software (Sciex). Incorporation of [*d*4]16:0 was calculated by combining the values of [*d*4]16:0, [*d*4]18:0, and [*d*4]20:0 molecular species, the values of 18:1 and 20:1 were combined for 18:1 incorporation; the values of 18:2 and 20:2 were combined for 18:2 incorporation; the values of 18:3 and 20:3 were combined for 18:3 incorporation; and the incorporation of 20:4 was a stand-alone value.

The samples were introduced to the QTrap 4500 by direct injection to perform product scans to verify the fatty acids present in a particular molecular species. The ion source parameters for the negative mode product scan were: ion spray voltage, −4500 V; curtain gas, 10 psi; collision gas, medium; temperature, 270 °C; ion source gas 1, 10 psi; ion source gas 2, 15 psi; declustering potential, −40 V; and collision energy −50 V.

Fatty acid composition of human serum

Lipids were extracted from human serum (Millipore-Sigma) by the method of Bligh and Dyer (35), and fatty acid methyl esters were prepared using methanol/hydrochloric acid. The fatty acid methyl esters were analyzed by a Hewlett-Packard model 5890 gas chromatograph equipped with a flame ionization detector and separated on 30 m × 0.536 mm × 0.50-μm DB-225 capillary column. The injector was set at 250 °C, and the detector was at 300 °C. The temperature program was as followed: initial temperature of 70 °C for 2 min, rate of 20 °C/min for 5 min (final 170 °C), rate of 2 °C/min for 10 min (final 190 °C), hold at 190 °C for 5 min, rate of 2 °C/min for 15 min (final 220 °C), hold at 220 °C for 5 min. The identity of fatty acid methyl esters was determined by comparing their retention times with fatty acid methyl ester standards (Matreya). The composition was expressed as weight percentages.

FA kinase assay

FA kinase assays contained 0.1 M Tris-HCl (pH 7.5), 10 mM ATP, 20 mM $MgCl_2$, 0.1% Brij-58, 20 μM [^{14}C]16:0, [^{14}C]18:1, or [^{14}C]18:2, 0.2 μM FakA, and the indicated concentrations of purified FakB proteins in a total volume of 60 μl. Tubes were incubated at 37 °C for 5 min before acetic acid (0.6%) was added and 40 μl was pipetted onto a DE81 Whatman filter paper disc and discs were washed three times, 20 min each, in ethanol containing acetic acid (1%). Discs were dried and counted by scintillation counting. Apparent K_m values were determined performing a nonlinear regression and using the Michaelis-Menten equation.

FA competition assays contained 10 μM FakB1, 1 μM FakB2, or 1 μM FakB3, 20 μM of the preferred radiolabeled substrate ([^{14}C]16:0, [^{14}C]18:1, or [^{14}C]18:2) plus 80 μM of one unlabeled FA (16:0, 18:1, 18:2, 18:3, or 20:4). The reaction conditions were the same as above with the exception that the total volume of the reaction was 100 μl. Eighty microliters was spotted onto DE81 Whatman filter paper discs. Discs were washed three times with an ethanol/acetic acid (1%) mixture for 20 min each wash. Discs were dried and counted by scintillation counting. Experiments were each performed three times in duplicate.

Protein crystallization and structure determination

All crystals were grown using the hanging drop method from pre-formed *Sp*FakB-FA complexes that were prepared as previously described (5). Specific crystallization conditions are as follows: *Sp*FakB1(16:0) and *Sp*FakB1(14:0), 0.1 M MES (pH 6.5) and 30% (w/v) PEG4000; *Sp*FakB2(C18:1Δ9), 0.1 M sodium HEPES (pH 7.5), 10% (v/v) isopropyl alcohol, 20% (w/v) PEG 4000; *Sp*FakB2(18:1Δ11), 18% (w/v) PEG 3350, 4.8% (v/v) 2-propanol, 0.1 M CAPSO, 17% (v/v) PEG400; *Sp*FakB3(18:2), 0.1 M sodium acetate (pH 4.6), and 8% (w/v) PEG4000. For data collection, crystals were cryoprotected in mother liquor containing 25% glycerol prior to flash freezing in liquid nitrogen. Glycerol could not be used as cryoprotectant with *Sp*FakB1(14:0) crystals because they immediately cracked and dissolved. Instead, crystals were briefly immersed in a 1:1 mixture of paraffin oil/Paratone N prior to freezing. X-ray diffraction data (180°) were collected at SER-CAT beamlines 22-ID and 22-BM at the APS (Argonne National Laboratory). Data were integrated with XDS (36, 37) and scaled and merged using AIMLESS/CCP4 (38). The *Sp*FakB1 and *Sp*FakB2 structures were determined by molecular replacement using the *Sa*FakB1 and *Sa*FakB2 structures as search models. For *Sp*FakB3, the structure was eventually determined using a structurally related protein from *Eubacterium eligens* (PDB ID 3FDJ) as the search model. Molecular replacement procedures were performed using MOLREP (39), MODBASE (40), MrBUMP/CCP4 (41), and PHASER (42). The FA 3-dimensional coordinates were designed using AVOGADRO (28) and the .cif dictionaries of restraints were generated with PHENIX.ELBOW (43). Multiple cycles of manual and real space refinement were performed using COOT (44), REFMAC (39), and PHENIX.REFINE (45). The final models of *Sp*FakB1, *Sp*FakB2, and *Sp*FakB3 contained 1, 2, and 2 monomers per asymmetric unit, respectively. 5% of the reflections was excluded from the refinement process for calculation of R_{free}. Structural statistics are presented in Table 2.

Author contributions—J. M. G., S. W. W., and C. O. R. conceptualization; J. M. G., M. G. C., M. W. F., S. W. W., and C. O. R. formal analysis; J. M. G., M. G. C., and M. W. F. investigation; J. M. G., M. G. C., and M. W. F. methodology; J. M. G. and C. O. R. writing-original draft; J. M. G., M. G. C., M. W. F., S. W. W., and C. O. R. writing-review and editing; M. G. C. data curation; M. G. C. visualization; S. W. W. validation; C. O. R. supervision; C. O. R. funding acquisition; C. O. R. project administration.

Acknowledgments—We thank Pam Jackson for assistance with the molecular biology, Karen Miller for protein purification, and Hannah Rowe and Jason Rosch for advice and assistance in creating strain JMG1. Use of the Advanced Photon Source was supported by the U. S. Dept. of Energy, Office of Science, Office of Basic Energy Sciences, under Contract No. W-31-109-Eng-38.

References

1. Parsons, J. B., Broussard, T. C., Bose, J. L., Rosch, J. W., Jackson, P., Subramanian, C., and Rock, C. O. (2014) Identification of a two-component fatty acid kinase responsible for host fatty acid incorporation by *Staphylococcus aureus*. *Proc. Natl. Acad. Sci. U.S.A.* **111,** 10532–10537 CrossRef
2. Yao, J., and Rock, C. O. (2015) How bacterial pathogens eat host lipids: Implications for the development of fatty acid synthesis therapeutics. *J. Biol. Chem.* **290,** 5940–5946 CrossRef Medline
3. Parsons, J. B., Frank, M. W., Subramanian, C., Saenkham, P., and Rock, C. O. (2011) Metabolic basis for the differential susceptibility of Gram-positive pathogens to fatty acid synthesis inhibitors. *Proc. Natl. Acad. Sci. U.S.A.* **108,** 15378–15383 CrossRef Medline
4. Parsons, J. B., Frank, M. W., Jackson, P., Subramanian, C., and Rock, C. O. (2014) Incorporation of extracellular fatty acids by a fatty acid kinase-dependent pathway in *Staphylococcus aureus*. *Mol. Microbiol.* **92,** 234–245 CrossRef Medline
5. Cuypers, M. G., Subramanian, C., Gullett, J. M., Frank, M. W., White, S. W., and Rock, C. O. (2019) Acyl chain selectivity and physiological roles of *Staphylococcus aureus* fatty acid-binding proteins. *J. Biol. Chem.* **294,** 38–49 CrossRef Medline
6. Lu, Y. J., and Rock, C. O. (2006) Transcriptional regulation of fatty acid biosynthesis in *Streptococcus pneumoniae*. *Mol. Microbiol.* **59,** 551–566 CrossRef Medline
7. Eckhardt, T. H., Skotnicka, D., Kok, J., and Kuipers, O. P. (2013) Transcriptional regulation of fatty acid biosynthesis in *Lactococcus lactis*. *J. Bacteriol.* **195,** 1081–1089 CrossRef Medline
8. Faustoferri, R. C., Hubbard, C. J., Santiago, B., Buckley, A. A., Seifert, T. B., and Quivey, R. G., Jr. (2015) Regulation of fatty acid biosynthesis by the global regulator CcpA and the local regulator FabT in *Streptococcus mutans*. *Mol. Oral. Microbiol.* **30,** 128–146 CrossRef
9. Zhu, L., Zou, Q., Cao, X., and Cronan, J. E. (2019) *Enterococcus faecalis* encodes an atypical auxiliary acyl carrier protein required for efficient regulation of fatty acid synthesis by exogenous fatty acids. *MBio* **10,** e00577-19 Medline
10. Jerga, A., and Rock, C. O. (2009) Acyl-acyl carrier protein regulates transcription of fatty acid biosynthetic genes via the FabT repressor in *Streptococcus pneumoniae*. *J. Biol. Chem.* **284,** 15364–15368 Medline
11. Brinster, S., Lamberet, G., Staels, B., Trieu-Cuot, P., Gruss, A., and Poyart, C. (2009) Type II fatty acid synthesis is not a suitable antibiotic target for Gram-positive pathogens. *Nature* **458,** 83–86 CrossRef Medline
12. Broussard, T. C., Miller, D. J., Jackson, P., Nourse, A., White, S. W., and Rock, C. O. (2016) Biochemical roles for conserved residues in the bacterial fatty acid-binding protein family. *J. Biol. Chem.* **291,** 6292–6303 CrossRef Medline
13. Tatituri, R. V., Brenner, M. B., Turk, J., and Hsu, F. F. (2012) Structural elucidation of diglycosyl diacylglycerol and monoglycosyl diacylglycerol from *Streptococcus pneumoniae* by multiple-stage linear ion-trap mass spectrometry with electrospray ionization. *J. Mass Spectrom.* **47,** 115–123 CrossRef Medline
14. Delekta, P. C., Shook, J. C., Lydic, T. A., Mulks, M. H., and Hammer, N. D. (2018) *Staphylococcus aureus* utilizes host-derived lipoprotein particles as sources of exogenous fatty acids. *J. Bacteriol.* **200,** e00728-17 Medline
15. Kim, G. L., Luong, T. T., Park, S. S., Lee, S., Ha, J. A., Nguyen, C. T., Ahn, J. H., Park, K. T., Paik, M. J., Suhkneung, Pyo, Briles, D. E., and Rhee, D. K. (2017) Inhibition of autolysis by lipase LipA in *Streptococcus pneumoniae* sepsis. *Mol. Cells* **40,** 935–944 Medline
16. Schulze-Gahmen, U., Pelaschier, J., Yokota, H., Kim, R., and Kim, S. H. (2003) Crystal structure of a hypothetical protein, TM841 of *Thermotoga*

maritima, reveals its function as a fatty acid-binding protein. *Proteins* **50,** 526–530 CrossRef Medline
17. Nan, J., Zhou, Y., Yang, C., Brostromer, E., Kristensen, O., and Su, X. D. (2009) Structure of a fatty acid-binding protein from *Bacillus subtilis* determined by sulfur-SAD phasing using in-house chromium radiation. *Acta Crystallogr. D Biol. Crystallogr.* **65,** 440–448 CrossRef Medline
18. Parsons, J. B., and Rock, C. O. (2013) Bacterial lipids: metabolism and membrane homeostasis. *Prog. Lipid Res.* **52,** 249–276 CrossRef Medline
19. Yao, J., and Rock, C. O. (2013) Phosphatidic acid synthesis in bacteria. *Biochim. Biophys. Acta* **1831,** 495–502 CrossRef Medline
20. Storch, J., and Corsico, B. (2008) The emerging functions and mechanisms of mammalian fatty acid-binding proteins. *Annu. Rev. Nutr.* **28,** 73–95 CrossRef Medline
21. Storch, J., and McDermott, L. (2009) Structural and functional analysis of fatty acid-binding proteins. *J. Lipid Res.* **50,** S126–131 CrossRef Medline
22. He, Y., Yang, X., Wang, H., Estephan, R., Francis, F., Kodukula, S., Storch, J., and Stark, R. E. (2007) Solution-state molecular structure of apo and oleate-liganded liver fatty acid-binding protein. *Biochemistry* **46,** 12543–12556 CrossRef Medline
23. Hodsdon, M. E., and Cistola, D. P. (1997) Ligand binding alters the backbone mobility of intestinal fatty acid-binding protein as monitored by ^{15}N NMR relaxation and ^{1}H exchange. *Biochemistry* **36,** 2278–2290 CrossRef Medline
24. Hodsdon, M. E., and Cistola, D. P. (1997) Discrete backbone disorder in the nuclear magnetic resonance structure of apo intestinal fatty acid-binding protein: implications for the mechanism of ligand entry. *Biochemistry* **36,** 1450–1460 CrossRef Medline
25. Sacchettini, J. C., Gordon, J. I., and Banaszak, L. J. (1989) Refined apoprotein structure of rat intestinal fatty acid binding protein produced in *Escherichia coli*. *Proc. Natl. Acad. Sci. U.S.A.* **86,** 7736–7740 CrossRef
26. Richieri, G. V., Ogata, R. T., Zimmerman, A. W., Veerkamp, J. H., and Kleinfeld, A. M. (2000) Fatty acid binding proteins from different tissues show distinct patterns of fatty acid interactions. *Biochemistry* **39,** 7197–7204 CrossRef Medline
27. Tian, W., Chen, C., Lei, X., Zhao, J., and Liang, J. (2018) CASTp 3.0: computed atlas of surface topography of proteins. *Nucleic Acids Res.* **46,** W363–W367 CrossRef Medline
28. Prinsen, C. F., and Veerkamp, J. H. (1996) Fatty acid binding and conformational stability of mutants of human muscle fatty acid-binding protein. *Biochem. J.* **314,** 253–260 CrossRef Medline
29. Corsico, B., Cistola, D. P., Frieden, C., and Storch, J. (1998) The helical domain of intestinal fatty acid binding protein is critical for collisional transfer of fatty acids to phospholipid membranes. *Proc. Natl. Acad. Sci. U.S.A.* **95,** 12174–12178 CrossRef Medline
30. Falomir-Lockhart, L. J., Laborde, L., Kahn, P. C., Storch, J., and Córsico, B. (2006) Protein-membrane interaction and fatty acid transfer from intestinal fatty acid-binding protein to membranes: support for a multistep process. *J. Biol. Chem.* **281,** 13979–13989 CrossRef Medline
31. Pang, Y. Y., Schwartz, J., Thoendel, M., Ackermann, L. W., Horswill, A. R., and Nauseef, W. M. (2010) agr-Dependent interactions of *Staphylococcus aureus* USA300 with human polymorphonuclear neutrophils. *J. Innate. Immun.* **2,** 546–559 CrossRef Medline
32. Subramanian, C., Frank, M. W., Batte, J. L., Whaley, S. G., and Rock, C. O. (2019) Oleate hydratase from *Staphylococcus aureus* protects against palmitoleic acid, the major antimicrobial fatty acid produced by mammalian skin. *J. Biol. Chem.* **294,** 9285–9294 CrossRef Medline
33. Wurch, T., Lestienne, F., and Pauwels, P. J. (1998) A modified overlap extension PCR method to create chimeric genes in the absence of restriction enzymes. *Biotechnol. Tech.* **12,** 653–657 CrossRef
34. Granok, A. B., Parsonage, D., Ross, R. P., and Caparon, M. G. (2000) The RofA binding site in *Streptococcus pyogenes* is utilized in multiple transcriptional pathways. *J. Bacteriol.* **182,** 1529–1540 CrossRef Medline
35. Bligh, E. G., and Dyer, W. J. (1959) A rapid method of total lipid extraction and purification. *Can. J. Biochem. Physiol.* **37,** 911–917 CrossRef Medline
36. Kabsch, W. (2010) XDS. *Acta Crystallogr. D Biol. Crystallogr.* **66,** 125–132 CrossRef Medline
37. Kabsch, W. (2010) Integration, scaling, space-group assignment and post-refinement. *Acta Crystallogr. D Biol. Crystallogr.* **66,** 133–144 CrossRef Medline
38. Evans, P. R., and Murshudov, G. N. (2013) How good are my data and what is the resolution? *Acta Crystallogr. D Biol. Crystallogr.* **69,** 1204–1214 CrossRef Medline
39. Murshudov, G. N., Vagin, A. A., and Dodson, E. J. (1997) Refinement of macromolecular structures by the maximum-likelihood method. *Acta Crystallogr. D Biol. Crystallogr.* **53,** 240–255 CrossRef Medline
40. Pieper, U., Webb, B. M., Dong, G. Q., Schneidman-Duhovny, D., Fan, H., Kim, S. J., Khuri, N., Spill, Y. G., Weinkam, P., Hammel, M., Tainer, J. A., Nilges, M., and Sali, A. (2014) ModBase, a database of annotated comparative protein structure models and associated resources. *Nucleic Acids Res.* **42,** D336–D346 CrossRef Medline
41. Keegan, R. M., and Winn, M. D. (2007) Automated search-model discovery and preparation for structure solution by molecular replacement. *Acta Crystallogr. D Biol. Crystallogr.* **63,** 447–457 CrossRef Medline
42. McCoy, A. J., Grosse-Kunstleve, R. W., Adams, P. D., Winn, M. D., Storoni, L. C., and Read, R. J. (2007) Phaser crystallographic software. *J. Appl. Crystallogr.* **40,** 658–674 CrossRef Medline
43. Adams, P. D., Afonine, P. V., Bunkóczi, G., Chen, V. B., Davis, I. W., Echols, N., Headd, J. J., Hung, L. W., Kapral, G. J., Grosse-Kunstleve, R. W., McCoy, A. J., Moriarty, N. W., Oeffner, R., Read, R. J., Richardson, D. C., Richardson, J. S., Terwilliger, T. C., and Zwart, P. H. (2010) PHENIX: a comprehensive Python-based system for macromolecular structure solution. *Acta Crystallogr. D Biol. Crystallogr.* **66,** 213–221 CrossRef Medline
44. Emsley, P., Lohkamp, B., Scott, W. G., and Cowtan, K. (2010) Features and development of Coot. *Acta Crystallogr. D Biol. Crystallogr.* **66,** 486–501 CrossRef Medline
45. Afonine, P. V., Grosse-Kunstleve, R. W., Echols, N., Headd, J. J., Moriarty, N. W., Mustyakimov, M., Terwilliger, T. C., Urzhumtsev, A., Zwart, P. H., and Adams, P. D. (2012) Towards automated crystallographic structure refinement with phenix.refine. *Acta Crystallogr. D Biol. Crystallogr.* **68,** 352–367 CrossRef Medline
46. Boles, B. R., Thoendel, M., Roth, A. J., and Horswill, A. R. (2010) Identification of genes involved in polysaccharide-independent *Staphylococcus aureus* biofilm formation. *PLoS ONE* **5,** e10146 CrossRef Medline
47. D'Elia, M. A., Pereira, M. P., Chung, Y. S., Zhao, W., Chau, A., Kenney, T. J., Sulavik, M. C., Black, T. A., and Brown, E. D. (2006) Lesions in teichoic acid biosynthesis in *Staphylococcus aureus* lead to a lethal gain of function in the otherwise dispensable pathway. *J. Bacteriol.* **188,** 4183–4189 CrossRef Medline
48. Ericson, M. E., Subramanian, C., Frank, M. W., and Rock, C. O. (2017) Role of fatty acid kinase in cellular lipid homeostasis and SaeRS-dependent virulence factor expression in *Staphylococcus aureus*. *mBio* **8,** e00988-17 Medline
49. LeBlanc, D. J., Lee, L. N., and Abu-Al-Jaibat, A. (1992) Molecular, genetic, and functional-analysis of the basic replicon of pva380–1, a plasmid of oral streptococcal origin. *Plasmid* **28,** 130–145 CrossRef Medline